

A study of various parameters of spherically curved phased arrays for noninvasive ultrasound surgery

Xiaobing Fan† and Kullervo Hynynen

Department of Radiology, Brigham and Women's Hospital, Harvard Medical School, Boston, MA 02115, USA

Received 19 October 1995

Abstract. The spherically curved square element phased array design for ultrasound surgery was studied in several of its important aspects. A method for determining the spatial limitations of the multiple-foci region was developed for spherically curved phased arrays. The effects on the ultrasound fields of varying the phases and the amplitudes at control points were investigated. It was found that the phases and the magnitudes of control points have an impact on the ultrasound field distributions. The effects of multiple-foci spacing, pulse duration, and maximum temperature on the size and shape of necrosed tissue were investigated. For a spherically curved phased array with an 8 cm radius of curvature, an $8.8 \times 8.8 \text{ cm}^2$ projected area, and a 1.5 MHz operating frequency, the minimum number of phased array elements that could produce the largest acceptable necrosed tissue volume was 256. The tissue volume necrosed during the sonication could be increased to approximately $1 \times 1 \times 3 \text{ cm}^3$ with this array.

1. Introduction

Phased arrays have shown great potential as ultrasound applicators for deep localized hyperthermia (Do-Huu and Hartemann 1981, Ocheltree *et al* 1984, Cain and Umemura 1986, Benkeser *et al* 1987, Ebbini *et al* 1988, Ebbini and Cain 1991a, Yoon 1991), and for generating necrosed tissue volumes in ultrasound surgery (Fan and Hynynen 1995, 1996). Spherically curved phased arrays are capable of significantly increasing the necrosed tissue volume when compared with a similar single focused transducer. The ability to control the necrosed tissue volume in ultrasound surgery gives the phased array a unique advantage over the other methods of enlarging the necrosed tissue volume. Fan and Hynynen (1995) demonstrated that a phased array system with a small number of elements can be used to control the focal spot size for ultrasound surgery. However, the 16-element phased array can only produce very limited useful field distribution. The increased focal spot size is important when large tumours are treated. Fan and Hynynen (1996) also demonstrated that phased arrays can offer significantly shorter treatment times than similar spherically curved transducers. However, the number of field patterns that produce different shapes or sizes of the necrosed tissue volume is limited by the number of phased array elements. To have more flexibility of field patterns, the number of the phased array elements has to increase, which results in more complex electronic circuits that are required to drive the array. When the size of the focus is increased, the ultrasound field intensity ratio between the tumour and

† Present address: Radiation Oncology Center, Washington University School of Medicine, Saint Louis, MO 63110, USA.

skin will decrease. This will cause near-field heating and normal tissue damage. Therefore, there is a practical limit of the focal volume for a given array.

A theoretical study on the design of spherically curved phased arrays is presented in this article. Various sonication patterns and array parameters were investigated to evaluate their potential for ultrasound surgery. In addition, the effect of increasing the number of array elements was demonstrated. These studies illustrated the great flexibility of phased arrays for controlling the size and shape of the necrosed tissue volume.

2. Materials and methods

2.1. Array dimensions

The theoretical phased arrays used in this study have a projected surface area of $8.8 \times 8.8 \text{ cm}^2$, an 8 cm radius of curvature, and an operating frequency of 1.5 MHz. The number of array elements varied between 16, 64, 256, and 400. A diagram of the phased array design and the coordinate system used in this study is shown in figure 1.

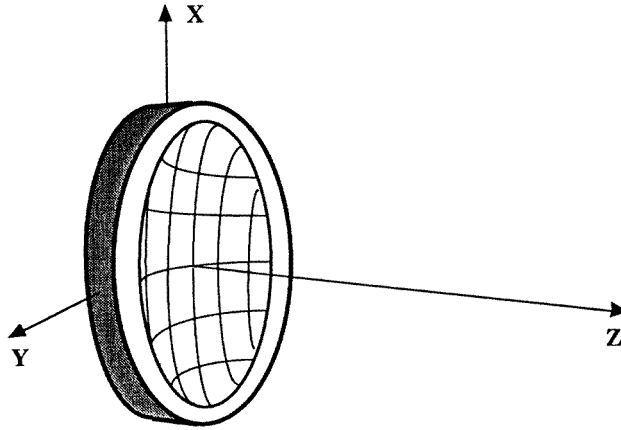


Figure 1. A diagram of the phased array design and the coordinate system used in this study.

2.2. Ultrasonic field calculations

The pressure field due to a N -element spherically curved ultrasound phased array can be evaluated by the Rayleigh–Sommerfeld integral (O’Neil 1949). For M field points, the pressure is given by

$$p_m = \sum_{n=1}^N u_n h_{mn} \quad (m = 1, 2, \dots, M) \quad (1)$$

and

$$h_{mn} = \frac{i\rho ck}{2\pi} \int_{S_n} \frac{e^{-ikr_{mn}}}{r_{mn}} dS_n \quad (2)$$

where $i = \sqrt{-1}$, ρ is the density of medium, c is the speed of sound, k is the wave number, $u_n = A_n e^{i(\omega t + \theta_n)}$ is the complex excitation of the n th element with amplitude A_n and phase

θ_n , r_{mn} is the distance from a point (x_n, y_n, z_n) on the n th element to the field point of interest (x_m, y_m, z_m) , and S_n is the area of the n th element.

By employing matrix notation, expression (1) can be written as

$$\mathbf{p} = \mathbf{H}\mathbf{u} \tag{3}$$

where

$$\mathbf{p} = \begin{pmatrix} p_1 \\ p_2 \\ \vdots \\ p_M \end{pmatrix} \quad \mathbf{H} = \begin{pmatrix} h_{11} & h_{12} & \dots & h_{1N} \\ h_{21} & h_{22} & \dots & h_{2N} \\ \vdots & \vdots & \ddots & \vdots \\ h_{M1} & h_{M2} & \dots & h_{MN} \end{pmatrix} \quad \mathbf{u} = \begin{pmatrix} u_1 \\ u_2 \\ \vdots \\ u_N \end{pmatrix}.$$

The elements of matrix \mathbf{H} are evaluated by numerical integration using expression (2). In attenuated medium, the power deposition for the desired volume is given by

$$Q(x, y, z) = \mu_{abs} \frac{|p_m(x, y, z)|^2}{Z} \quad (m = 1, 2, \dots, M)$$

where μ_{abs} is the absorption coefficient and $Z = \rho c$ is the impedance of the medium. The effect of the medium attenuation is taken into account by replacing $e^{-ikr_{mn}}$ with $e^{-ik_c r_{mn}}$. Here $k_c = k - i\alpha$ is the complex wave number, and α is the attenuation coefficient of the medium.

2.3. Methods of determining the phases and amplitudes of control points

For a given set of control points, the excitation source vector \mathbf{u} can be obtained from equation (3)

$$\mathbf{u} = \mathbf{H}^\dagger \mathbf{p} \tag{4}$$

where \mathbf{H}^\dagger is the pseudoinverse matrix of \mathbf{H} . For selected control points at desired focal positions, both the magnitudes and the phases have to be specified in order to use equation (4) because the pressures at these points are complex numbers. Therefore, it is necessary to determine the phase and the amplitude of the pressure at the control points. Two methods were investigated here.

The first method, introduced by Ebbini and Cain (1991a), is used to calculate the amplitude and phase settings from selected control points so that the gain is the maximum. In this study, a different view of this method is given in the following.

Using the same terminology as Ebbini and Cain, the gain is defined by

$$G = \frac{\mathbf{p}^* \mathbf{p}}{\mathbf{u}^* \mathbf{u}} \tag{5}$$

where \mathbf{p}^* and \mathbf{u}^* are the complex conjugate transposes of \mathbf{p} and \mathbf{u} , respectively. By utilizing singular value decomposition, matrix \mathbf{H} and its pseudoinverse matrix \mathbf{H}^\dagger can be given in the forms (Golub and Kahan 1965)

$$\mathbf{H} = \mathbf{X}\mathbf{S}\mathbf{Y}^* \quad \text{and} \quad \mathbf{H}^\dagger = \mathbf{Y}\hat{\mathbf{S}}\mathbf{X}^* \tag{6}$$

where \mathbf{X} and \mathbf{Y} are unitary matrices, and \mathbf{S} is a rectangular matrix of the same size as \mathbf{H} with nonnegative real diagonal entries $s_1 \geq s_2 \geq \dots \geq s_M$ (singular values of \mathbf{H}). $\hat{\mathbf{S}}$ is obtained from \mathbf{S} by replacing each positive diagonal entry by its reciprocal. Using equations (4) and (6), the following formula can be obtained

$$\mathbf{u}^* \mathbf{u} = \mathbf{p}^* \mathbf{X}\hat{\mathbf{S}}^* \mathbf{Y}^* \mathbf{Y}\hat{\mathbf{S}} \mathbf{X}^* \mathbf{p} = \mathbf{p}^* \mathbf{X}\hat{\mathbf{S}}^* \hat{\mathbf{S}} \mathbf{X}^* \mathbf{p}.$$

Because the matrix $\hat{\mathbf{S}}$ has a special structure, $\hat{\mathbf{S}}^*\hat{\mathbf{S}}$ is a diagonal matrix, denoted as $\hat{\Lambda}$, with diagonal entries $\hat{\lambda}_m = s_m^{-2}$ ($m = 1, 2, \dots, M$). By defining a new matrix $\mathbf{v} = \mathbf{X}^*\mathbf{p}$, it follows that $\mathbf{p} = \mathbf{X}\mathbf{v}$, and the gain is then given in the form

$$G = \frac{\mathbf{p}^*\mathbf{p}}{\mathbf{p}^*\mathbf{X}\hat{\Lambda}\mathbf{X}^*\mathbf{p}} = \frac{\mathbf{v}^*\mathbf{v}}{\mathbf{v}^*\hat{\Lambda}\mathbf{v}} = \frac{\sum_{m=1}^M |\mathbf{v}_m|^2}{\sum_{m=1}^M \hat{\lambda}_m |\mathbf{v}_m|^2}.$$

From the above expression, it can be seen that the gain is bounded by the minimum and the maximum square of the singular values of the matrix \mathbf{H} ,

$$s_M^2 = \frac{1}{\hat{\lambda}_M} \leq G \leq \frac{1}{\hat{\lambda}_1} = s_1^2.$$

\mathbf{X} was defined as $[\mathbf{x}_1, \mathbf{x}_2, \dots, \mathbf{x}_M]$, where \mathbf{x}_m ($m = 1, 2, \dots, M$) is the column vector of \mathbf{X} . When $\mathbf{v}^* = (1, 0, \dots, 0)$, i.e. $\mathbf{p} = \mathbf{x}_1$, the gain is equal to the maximum value s_1^2 . Therefore, the phases and the amplitudes of the first column vector of \mathbf{X} can be used as control points to perform the inverse calculation so that the gain is maximized. It is important to note that the magnitude of the components of \mathbf{x}_1 may not be constant. If it is necessary for the magnitudes of the control points to be the same but the magnitudes of the components in \mathbf{x}_1 are not the same, then the gain is close to the square of the largest singular value.

The second method of determining the phases and amplitudes of the control points was used by Fan and Hynynen (1995). Normally the control points were selected on a plane at a desired focal position. All the points were evenly distributed on circles or squares with centres on the central axis. The phases of the control points on each circle or square were chosen out of phase such that the phase rotated around the central axis (this is similar to the phase rotation used in the sector-vortex array by Cain and Umemura (1986)). The magnitudes of the control points were chosen to be the same for all the points which were equidistant from the central axis. This method of phase and amplitude selection will produce destructive interference on the central axis and minimize undesired peaks on the central axis. In the following studies, unless otherwise specified, the control points were selected on a square lattice in the focal plane. Any four adjacent points forming a square and having a 90° phase difference between adjacent points were used for the phase rotation method.

2.4. Multiple-foci boundary and spacing determinations

To enlarge the necrosed tissue volume with multiple foci, the control points should be distributed over a large area in the focal plane. For a given phased array, there is a limited region in the focal plane in which the multiple foci can be generated. In order to avoid selecting control points outside this limited region, the region should be known for a given array. The setting of the excitation sources with phases of zero and π alternating on the elements, and uniform magnitudes, was used to determine the limitation. The reason for using this kind of phase distribution was that the maximum phase shift between adjacent elements is π .

In order to produce multiple foci at the desired locations of the control points, the number of control points must be less than the number of phased array elements. The spacing between the adjacent control points will determine the total number of control points required to cover a certain area. If the spacing is too large, the necrosed tissue may not be united. If the spacing is too small, the total number of control points will be too large. Four foci in the focal plane located on the corners of a square generated by using a 64-element phased array were used to study the spacing. The study was done by varying the focus spacing, the maximum temperature level and the pulse duration.

2.5. Electrical switching of multiple foci and scanning of a single focus

Electrical switching of multiple foci was used to partition the total number of control points into groups of multiple-foci patterns (Ebbini and Cain 1991b). Using phased arrays it is possible to enlarge the size of the necrosed tissue volume by varying the number of foci generated inside the tumour. The larger the number of control points used, the more likely it is that the ultrasound field will have unexpected hot spots. Therefore, the method of electrical switching of multiple foci inside a tumour volume is proposed to produce a cleaner ultrasound field. The ultrasound field and the size of the necrosed tissue were compared to those generated when the same number of foci were generated by a phased array at the same time.

Electrical scanning of a single focus consists of generating a few focal points sequentially in the target volume in a short time (Ebbini and Cain 1991a). The time required to generate each focus is so short that these focal points can be treated as multiple foci. The procedure is repeated multiple times during a sonication. The phase required to generate the single focus is directly calculated according to the distance between the point on the centre of the element to the field point of interest.

2.6. Temperature and thermal dose calculations

An approximate temperature response to the power deposition was predicted by the transient bioheat transfer equation (Pennes 1948). The thermal response was simulated in a homogeneous medium in this study. The homogeneous medium is a good assumption for the ultrasound surgery because of the small volume being treated. The thermal conductivity is approximately $0.5 \text{ W m}^{-1} \text{ }^\circ\text{C}$, the specific heat of tissue and blood is approximately $3770 \text{ J kg}^{-1} \text{ }^\circ\text{C}$ (Chato 1985), and the blood perfusion rate is less sensitive for a short ultrasound pulse (Billard *et al* 1990). A surface temperature of 37°C on the cube and an initial temperature of 37°C inside the cube were used as boundary and initial conditions for all of the computations. A numerical finite-difference method was employed to solve the partial differential equation. Ultrasound pulse durations of one, five, and ten seconds were used in this study.

The thermal dose calculation was based on the technique suggested by Sapareto and Dewey (1984). The accumulated thermal dose was calculated at a reference temperature by numerical integration under different temperature profiles. The necrosed tissue volume was estimated by the volume surrounded by an isothermal dose of 240 min at a reference temperature of 43°C . This technique has been found to be a reasonable model for prediction of tissue necroses induced by a focused transducer (Damianou and Hynynen 1993).

In the ultrasound surgery, water is used as a coupling medium between the array and tissue. The water-tissue interface was 3 cm from the array centre. The speed of sound and the density were 1500 m s^{-1} and 998 kg m^{-3} respectively for both media. These numbers are a reasonable choice because the impedance of soft tissue and water are very close to each other, and the effect of tissue layers on the ultrasound field is small and can be ignored (Fan and Hynynen 1992, 1994). The attenuation coefficient of the tissue was assumed to be $10 \text{ Np m}^{-1} \text{ MHz}^{-1}$. The thermal properties of the tissue are given in table 1.

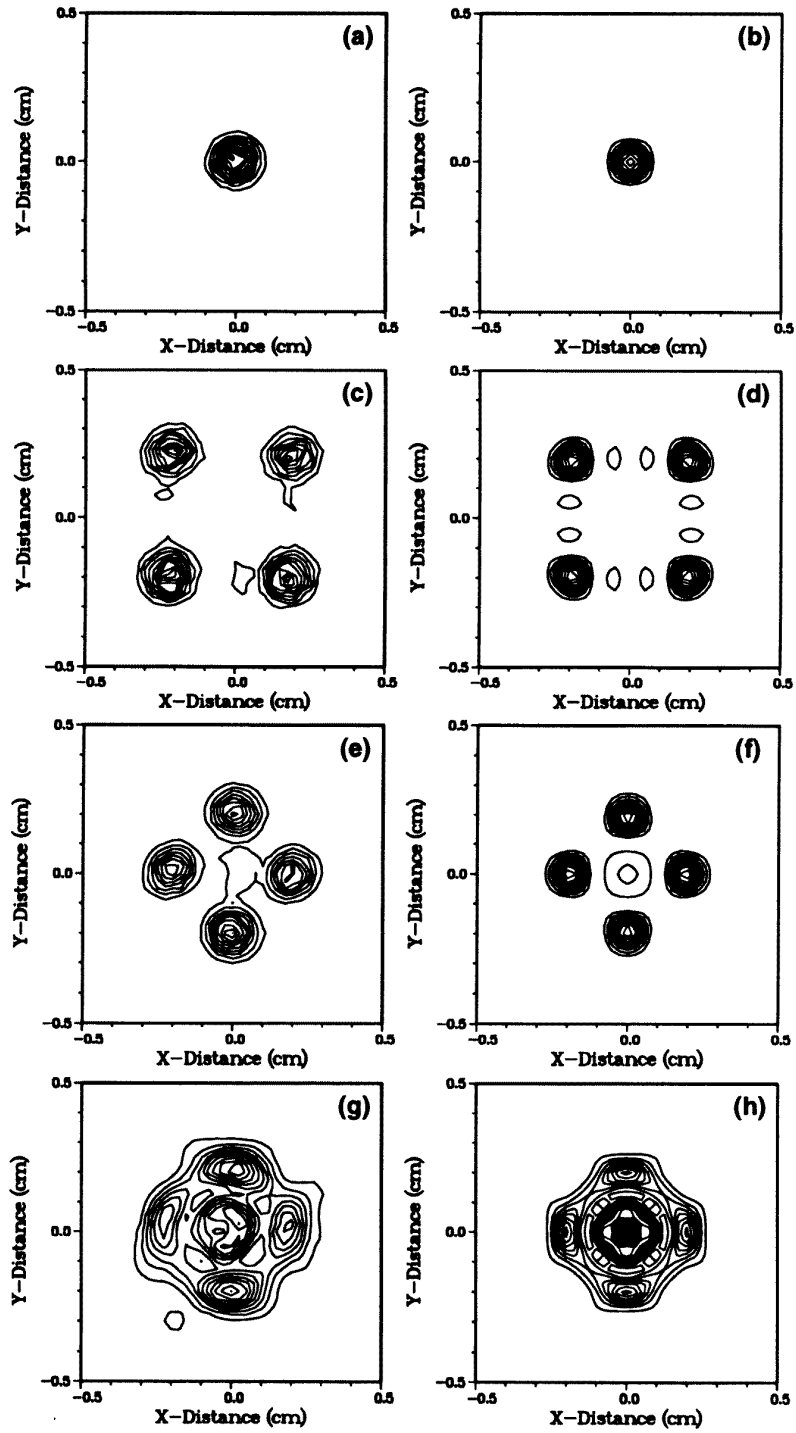
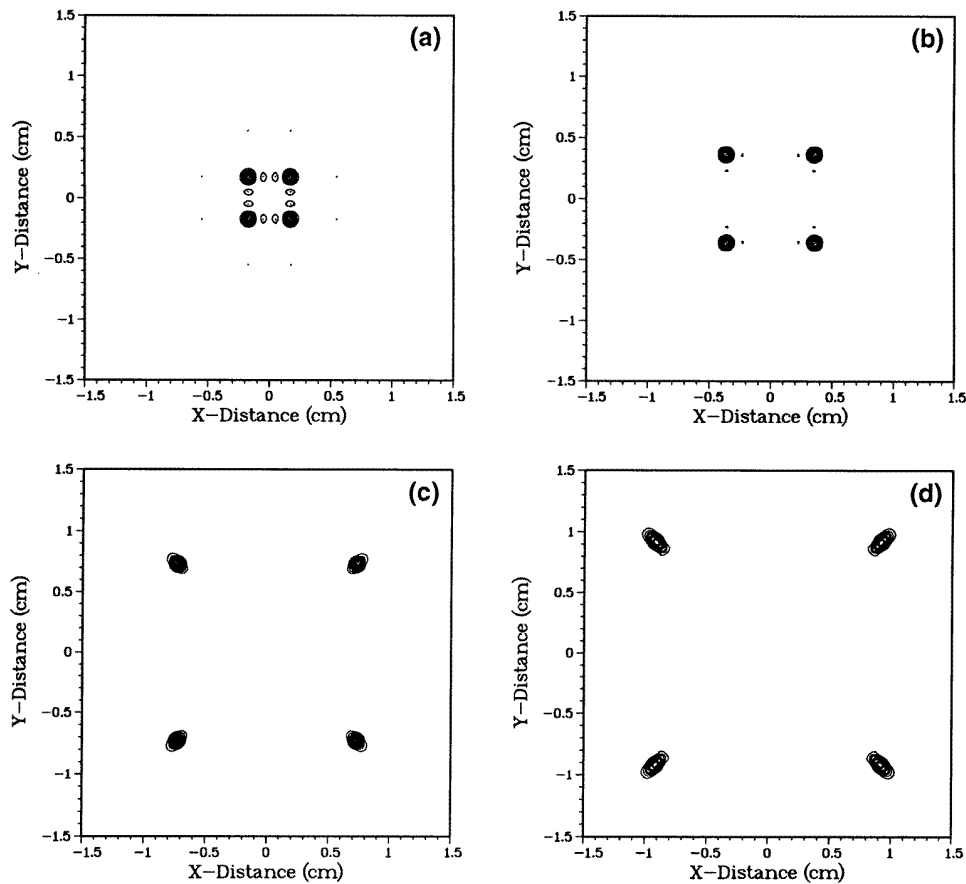


Figure 2. Contour plots of relative pressure amplitude squared distributions in the focal plane ($z = 8.0$ cm) for the 16-element array. Panels on the left are experimental results and on the right are simulation results.

Table 1. Thermal properties of tissue used in the simulations.

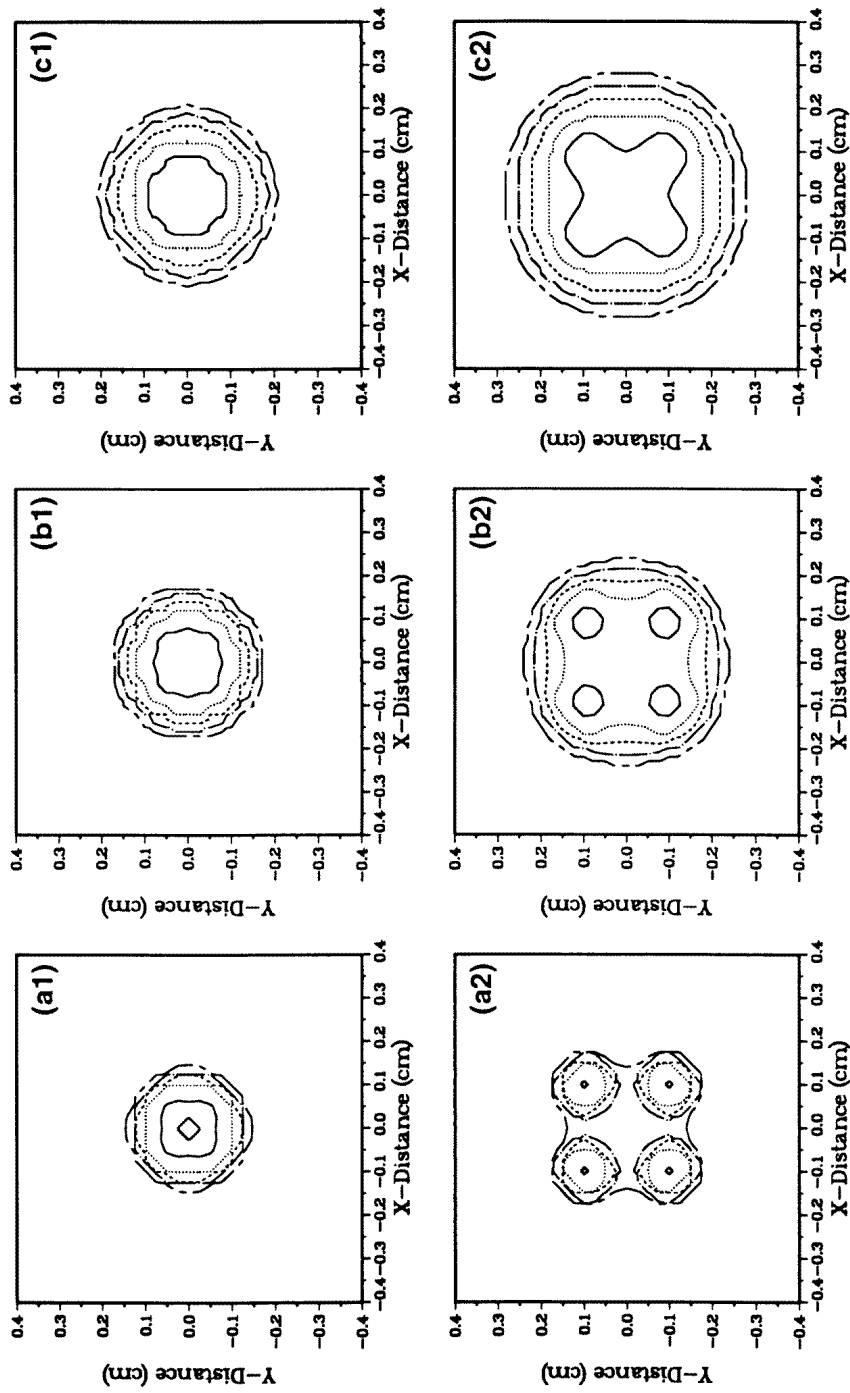
Parameter	Value	Units
Density of tissue	998	kg m^{-3}
Specific heat of tissue	3770	$\text{J kg}^{-1} \text{ } ^\circ\text{C}^{-1}$
Thermal conductivity of tissue	0.5	$\text{W m}^{-1} \text{ } ^\circ\text{C}^{-1}$
Blood perfusion rate	1	$\text{kg m}^{-3} \text{ s}^{-1}$
Specific heat of blood	3770	$\text{J kg}^{-1} \text{ } ^\circ\text{C}^{-1}$
Arterial blood temperature	37	$^\circ\text{C}$

**Figure 3.** Contour plots of relative pressure amplitude squared distributions in the focal plane ($z = 8.0$ cm). The numbers of phased array elements used in the simulations were (a) 16, (b) 64, (c) 256, and (d) 400.

3. Results

3.1. Comparison of experimental results with simulations

To better compare the experimental and simulated results of the phased array, a new spherically curved phased array was built. The new array is a 16-element array having



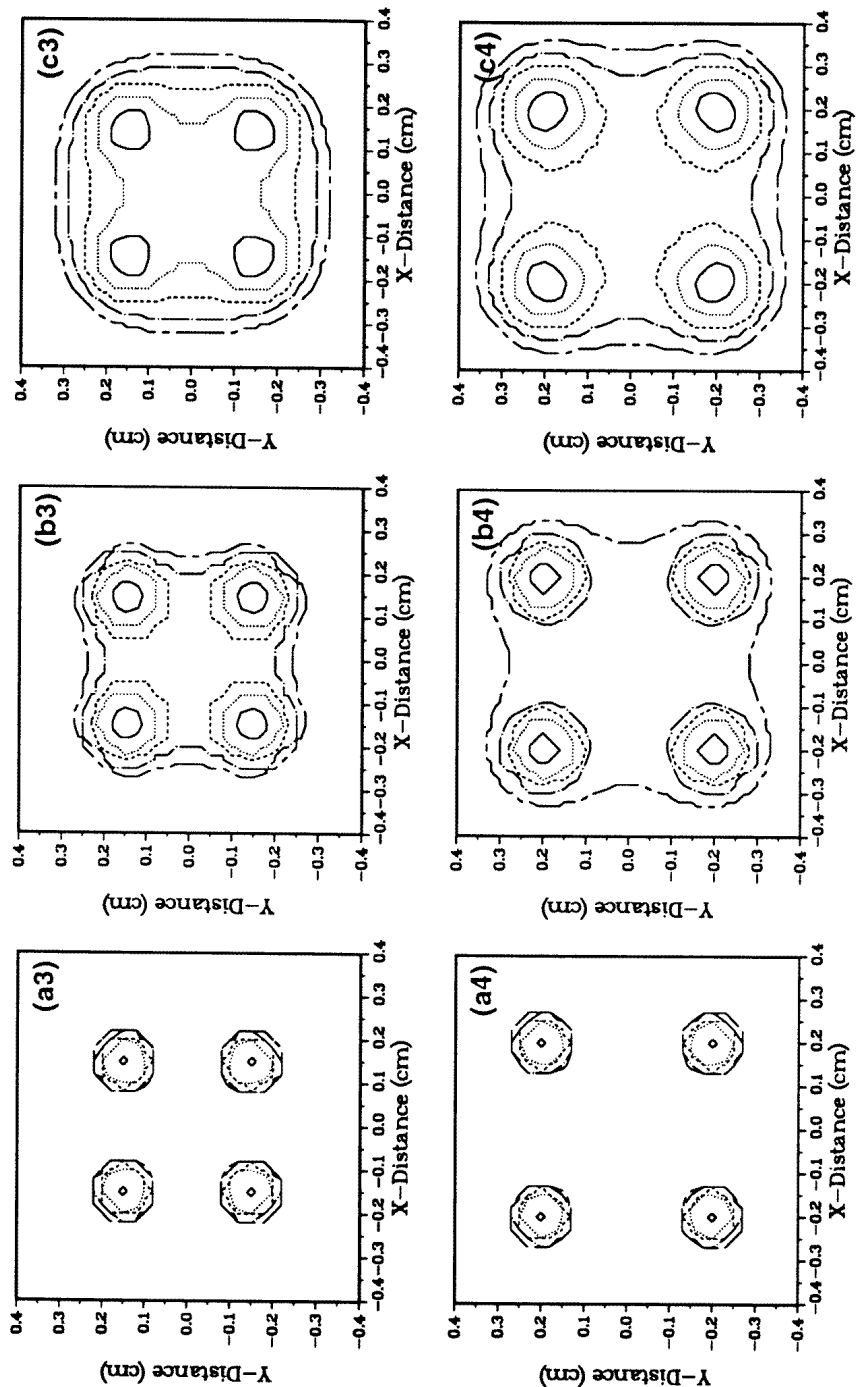


Figure 4. Isothermal dose lines at the focal plane for four different focus spacings. The focus spacings from top to bottom were 1 mm, 2 mm, 3 mm, and 4 mm, respectively. The pulse durations used in the calculations from left to right were 1 s, 5 s, and 10 s, respectively. The maximum temperature levels used in each figure were 100°C (chain-dashed line), 90°C (chain-dotted line), 80°C (dashed line), 70°C (dotted line), and 60°C (solid line).

a radius of curvature of 8 cm, an operating frequency of 1.45 MHz, and a projected element area of $2 \times 2 \text{ cm}^2$. The array construction and experimental technique can be found in Fan and Hynynen (1995). The contour plots of relative pressure amplitude squared distributions in the focal plane are shown in figure 2. There was good agreement between experimental and simulation results in the shape and the locations of foci. The simulation results tend to have narrower foci than the experimental results.

3.2. Simulation results

The results of multiple-foci boundary and spacing limitations are presented first. To determine the limitation region of the multiple foci, the method described in section 2.4 was used for the given arrays. Four foci located on the corners of a square (figure 3) in the focal plane ($z = 8.0 \text{ cm}$) were generated by using this special phase and amplitude setting. The area of the square linearly increased as the number of array elements increased.

The maximum multiple-foci spacing required to generate a united thermal dose was investigated by varying the spacing between the foci, the maximum temperature level, and pulse durations. Figure 4 shows the 240 min isothermal dose lines for four different focus spacings, five temperature levels, and three pulse durations for the 64-element array. Comparing these dose lines, it can be seen that the following three cases give acceptable size and shape of necrosed tissue: (I) 2 mm spacing, the maximum temperature above 80°C , 5 s pulse duration, (II) 2 mm spacing, the maximum temperature above 70°C , 10 s pulse duration, and (III) 3 mm spacing, the maximum temperature above 80°C , 10 s pulse duration. These results are for a low blood perfusion rate. For a high perfusion rate of $10 \text{ kg m}^{-3} \text{ s}^{-1}$ similar results were obtained (not shown here). In this case acceptable tissue necrosis was produced by (I) 2 mm spacing, the maximum temperature above 80°C , 5 s pulse duration, (II) 2 mm spacing, the maximum temperature above 70°C , 10 s pulse duration, and (III) 3 mm spacing, the maximum temperature above 90°C , 10 s pulse duration.

The phased array configuration for producing the largest necrosed tissue volumes with the smallest number of array elements was investigated next. The power deposition patterns with 16 foci generated by the 64-element array are shown in figures 5(a, b) (phase rotation method) and 5(e, f) (maximum gain method). The spacing between adjacent control points was 2 mm. The outer 12 foci were not clearly marked for this case. The corresponding lesion boundaries (240 min isothermal dose lines) for a 10 s pulse duration with four different maximum temperature levels are shown in figures 5(c, d) and 5(g, h), respectively. The acceptable shape of the necrosed tissue volume was only obtained for a maximum temperature of 70°C . For the same control points, the power deposition patterns and lesion boundaries produced by a 256-element array are shown in figure 6. The outer 12 foci were clearly obtained this time. The necrosed tissue volumes were all acceptable for the maximum temperature less than 100°C using the phase rotation method, but none were acceptable when the maximum gain method was used.

The power deposition patterns and lesion boundaries for 36 foci generated with 256- and 400-element arrays are shown in figure 7. A spacing between adjacent control points of 2 mm was used in the simulations. It can be seen that the necrosed tissue volumes generated by the 256-element array are larger than those generated by the 400-element array for the temperature levels less than 90°C . The necrosed tissue volume for the high temperature levels (90°C and 100°C) produced by the 256-element array were not acceptable, but they were acceptable for the 400-element array. However, the size of the necrosed tissue volumes (temperature levels 90°C and 100°C) for the 400-element array were not significantly larger than the necrosed tissue volumes for the 256-element array, especially in the lateral

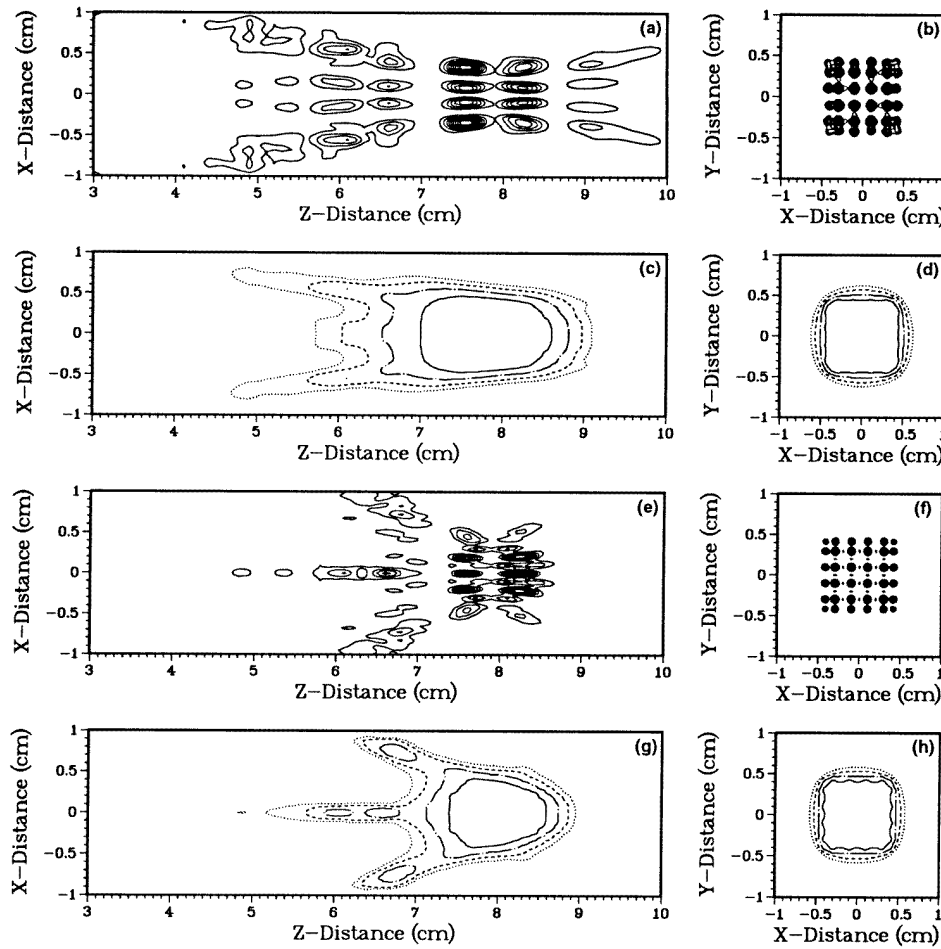


Figure 5. The power deposition pattern (a,b) and lesion boundaries (c,d) obtained with the 64-element array and the phase rotation method for the control points and the power deposition pattern (e,f) and lesion boundaries (g,h) obtained with the 64-element array and the maximum gain method. The spacing between adjacent control points was 2 mm. An ultrasound pulse duration of 10 s was used in the thermal dose calculations. The maximum temperature level was 100°C (dotted line), 90°C (dashed line), 80°C (chained line), and 70°C (solid line). The figures on the left are axial plane distributions ($y = 0$), and on the right are focal plane distributions ($z = 7.9$ cm).

direction. To further increase the necrosed tissue volume, 36 control points with a 3 mm spacing between control points were used in the simulations for the the same arrays. The power deposition patterns and lesion boundaries are shown in figure 8. It can be seen that the intensity ratio between the target and the interface dropped when an attempt was made to necrose a larger area. This resulted in unacceptable lesion shapes with both arrays.

Finally, to illustrate the advantage of switching a few groups of multiple foci or scanning a single focus to produce the necrosed tissue volume, the 256-element array was used in the following simulations. Figures 9(a)–(d) show the results obtained by switching two groups of four and 12 multiple-foci patterns to produce a total of 16 foci. The locations of the

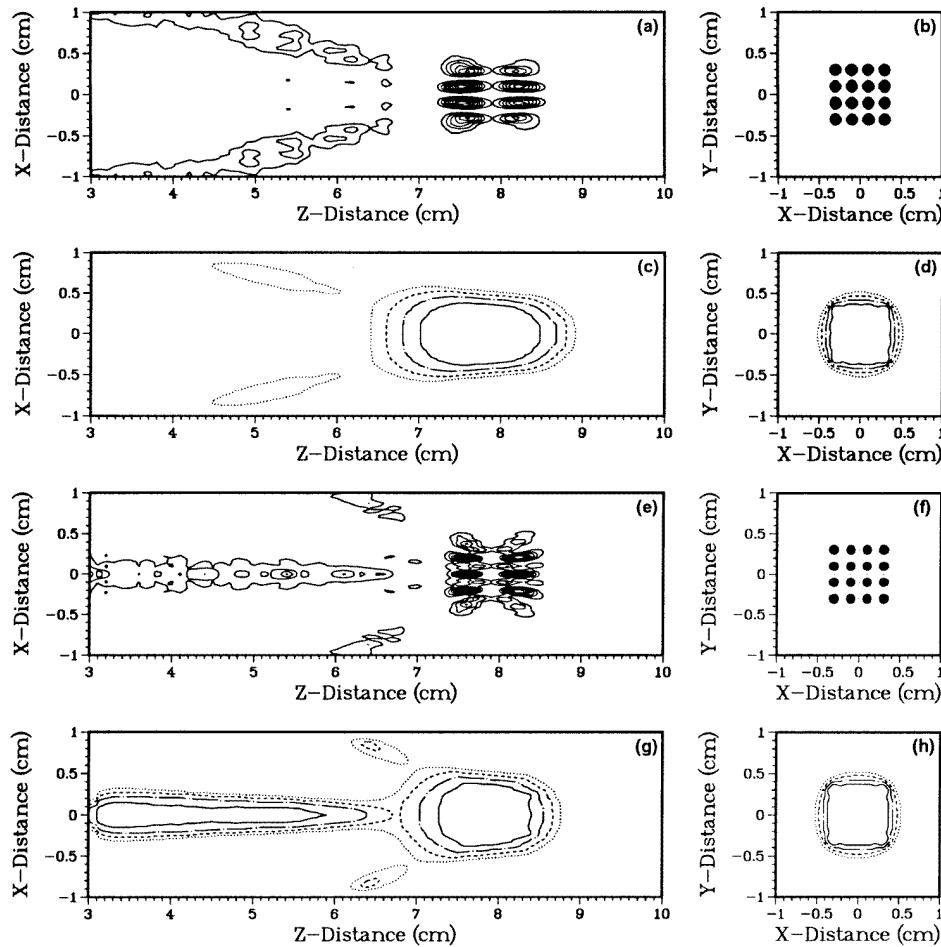


Figure 6. The power deposition pattern (a,b) and lesion boundaries (c,d) obtained with the 256-element array and the phase rotation method for the control points and the power deposition pattern (e,f) and lesion boundaries (g,h) obtained with the 256-element array and the maximum gain method. The spacing between adjacent control points was 2 mm. An ultrasound pulse duration of 10 s was used in the thermal dose calculations. The maximum temperature level was 100°C (dotted line), 90°C (dashed line), 80°C (chained line), and 70°C (solid line). The figures on the left are axial plane distributions ($y = 0$), and on the right are focal plane distributions ($z = 7.9$ cm).

control points were the same as in figure 6. Comparing these results with those shown in figure 6, it can be seen that the necrosed tissue volume slightly increased in the axial direction with less near field heating for high temperature levels. Figures 9(e)–9(h) show the results obtained by switching three groups of 4, 12, and 20 foci to generate a total of 36 foci. Comparing these results with figures 7(a)–(d), the necrosed tissue volumes significantly increased in the axial direction for the same temperature level. The power depositions and lesion boundaries produced by scanning a single focus are shown in figure 10. For the 16 foci case (figures 10(a)–(d)), the necrosed tissue volumes are almost the same as the case where the 16 foci were generated simultaneously, but with less near-field heating. For

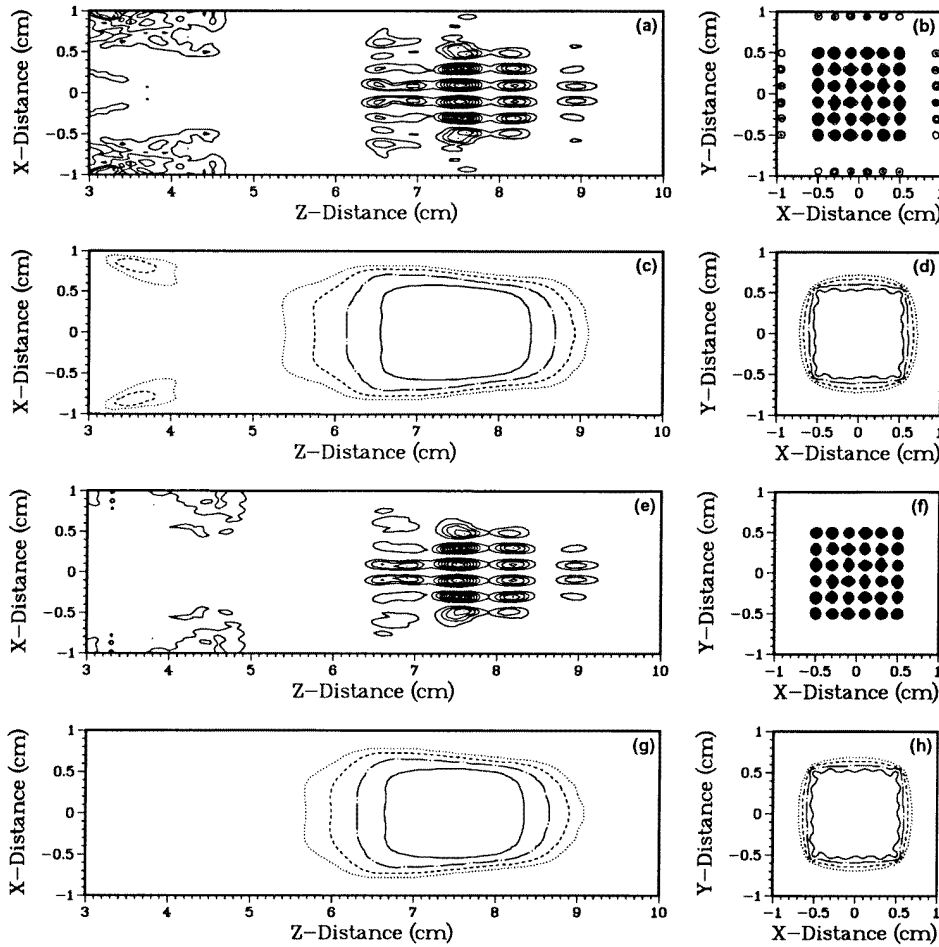


Figure 7. The power deposition pattern (a, b) and lesion boundaries (c, d) obtained with the 256-element array and the power deposition pattern (e, f) and lesion boundaries (g, h) obtained with the 400-element array. The spacing between adjacent control points was 2 mm. An ultrasound pulse duration of 10 s was used in the thermal dose calculations. The maximum temperature level was 100 °C (dotted line), 90 °C (dashed line), 80 °C (chained line), and 70 °C (solid line). The figures on the left are axial plane distributions ($y = 0$), and on the right are focal plane distributions ($z = 7.9$ cm).

the 36-foci case (figures 10(e)–10(h)), the necrosed tissue volumes increased in the axial direction, and produced more near-field heating compared to 36 foci generated by switching three groups of multiple foci.

4. Discussion

The feasibility of using spherically curved phased arrays in ultrasound surgery was investigated in this study. Spherically curved ultrasound phased arrays can be used to control the size of the necrosed tissue by generating multiple foci, by scanning a single focus, or by switching groups of multiple foci within the target volume. The results showed

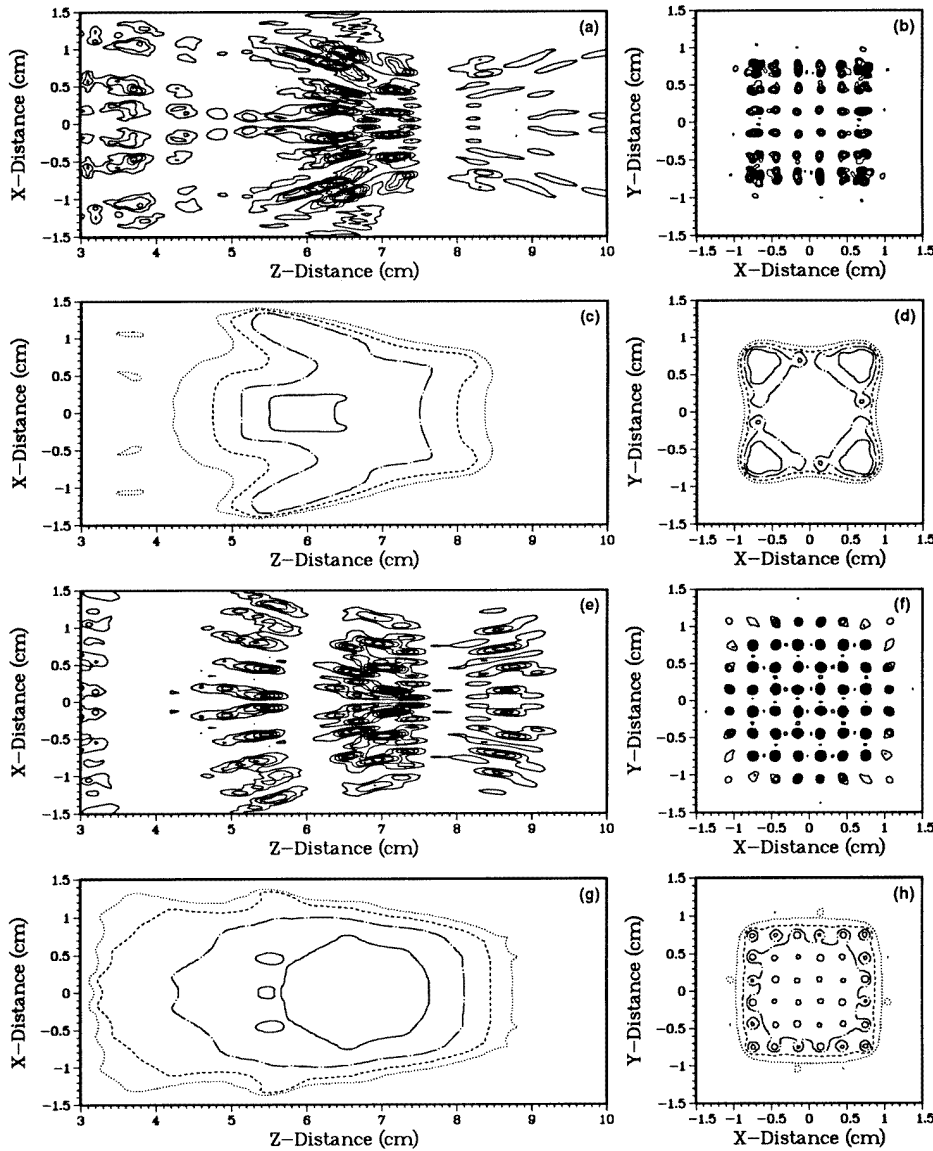


Figure 8. The power deposition pattern (a, b) and lesion boundaries (c, d) obtained with the 256-element array and the power deposition pattern (e, f) and lesion boundaries (g, h) obtained with the 400-element array. The spacing between adjacent control points was 3 mm. An ultrasound pulse duration of 10 s was used in the thermal dose calculations. The maximum temperature level was 100°C (dotted line), 90°C (dashed line), 80°C (chained line), and 70°C (solid line). The figures on the left are axial plane distributions ($y = 0$), and on the right are focal plane distributions ($z = 7.9$ cm).

that for a given phased array, there is a limit on the size of the necrosed tissue that can be generated due to the size of the aperture. For phased arrays having the same total projected area, radius of curvature, and operating frequency, there is number of array elements which will generate the largest necrosed tissue volume with the fewest number of elements. In

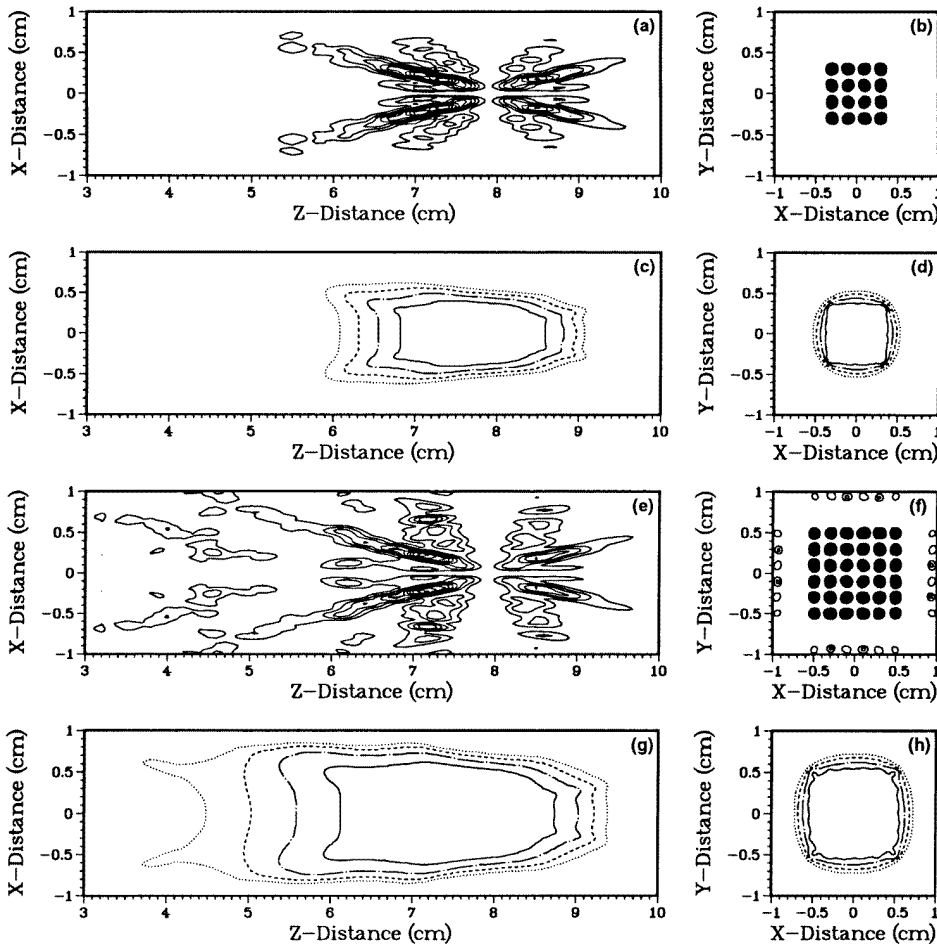


Figure 9. The power deposition pattern (a, b) and lesion boundaries (c, d) obtained by switching the two groups of multiple foci and the power deposition pattern (e, f) and lesion boundaries (g, h) obtained by switching the three groups of multiple foci. A 256-element phased array was used in the simulations. An ultrasound pulse duration of 10 s was used in the thermal dose calculations. The maximum temperature level was 100°C (dotted line), 90°C (dashed line), 80°C (chained line), and 70°C (solid line). The figures on the left are axial plane distribution ($y = 0$), and on the right are focal plane distributions ($z = 7.9$ cm).

this study, when control points were selected on an area larger than $10 \times 10 \text{ mm}^2$ in the focal plane, the intensity ratio between the focal plane and the interface decreased so much that normal tissue damage in front of the focus occurred. It appears that the 400-element array cannot generate a significantly larger necrosed tissue volume without increased near-field necrosis compared to the 256-element array when multiple foci are produced in the focal plane simultaneously. This is with the driving techniques tested here. Therefore, for phased arrays having a projection area of $8.8 \times 8.8 \text{ cm}^2$, a 8 cm radius of curvature, and an operating frequency of 1.5 MHz, the practical number of array elements appears to be around 256. However, the array with a larger number of elements allows more control over the field distributions and may prove to be more useful when different methods are used to

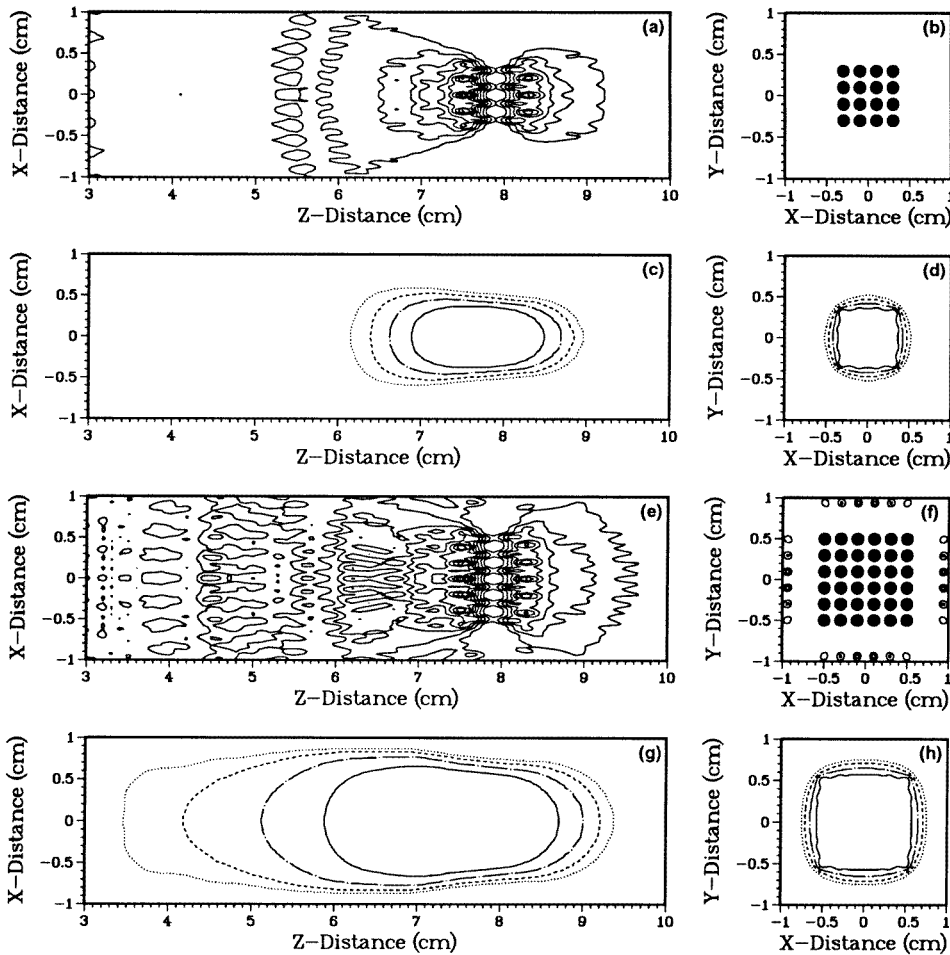


Figure 10. The power deposition patterns (a,b), (e,f), and lesion boundaries (c,d), (g,h), obtained by scanning a single focus with the 256-element phased array. An ultrasound pulse duration of 10 s was used in the thermal dose calculations. The maximum temperature level was 100 °C (dotted line), 90 °C (dashed line), 80 °C (chained line), and 70 °C (solid line). The figures on the left are axial plane distributions ($y = 0$), and on the right are focal plane distributions ($z = 7.9$ cm).

control the ultrasound field distributions.

The multiple-foci region in the focal plane for the spherically curved phased array can be determined by setting the excitation sources with alternating phases of zero and π and uniform amplitude. It is important to know the multiple-foci boundary so that the control points in the focal plane can be selected to produce desired focal points. When an attempt is made to generate multiple foci outside this region, the secondary foci will have a higher pressure field than the primary foci (Fan 1995). Therefore the multiple foci cannot be generated outside this limited region. The boundary limitation for a single focus produced by a phased array is smaller than for multiple-foci regions.

The maximum-foci spacing is dependent on the level of the maximum temperature, pulse duration, size of foci, and tissue perfusion. For the arrays used in this study, the

maximum-foci spacing was 2 mm for a maximum temperature of 80°C with a 5 s pulse or for a maximum temperature of 70°C with a 10 s pulse, and 3 mm for a maximum temperature of 90°C with a 10 s pulse. This maximum distance between the focal spots provides an acceptable results, however, it may not be the optimal way of necrosing the tissue.

The phases and amplitudes of the control points used in the inverse calculations have an impact on the ultrasound field associated with excitation sources. This can be understood by imagining the control points as point sources. These sources will produce interference fields according to the phases of these points. Both the phase rotation method for the control points and the maximum gain method can be used to determine the phases and the amplitudes of the excitation sources in the inverse calculations. The maximum gain method does not minimize acoustic interference in the near field. When control points were selected near the boundary of a multiple-foci region, the ultrasound field tended to have unwanted high-pressure peaks outside the target volume. In this case to avoid normal tissue damage, the necrosed tissue can only be obtained by lowering the maximum temperature.

Electrical switching of multiple foci or scanning of a single focus can be used to reduce the near-field heating and offer more control points than when all of the foci are generated simultaneously. These methods are useful when many focal points are required but only a small number of array elements are available. The ultrasound field sonication pattern for the given phased arrays was not optimized in this work, and further investigation needs to be done to decide what sonication method allows the treatment to be executed in a minimum amount of time.

Acknowledgments

This study was supported by NCI grant No CA 46627 and a grant from General Electric Company.

References

- Benkeser P J, Frizzell L A, Ocheltree K B and Cain C A 1987 A tapered phased array ultrasound transducer for hyperthermia treatment *IEEE Trans. Ultrason. Ferroelectr. Freq. Control* **UFFC-34** 446–53
- Billard B E, Hynynen K and Roemer R B 1990 Effects of physical parameters on high temperature ultrasound hyperthermia *Ultrasound Med. Biol.* **16** 409–20
- Cain C A and Umemura S 1986 Concentric-ring and sector vortex phased array applicators for ultrasound hyperthermia therapy *IEEE Trans. Microwave Theory Technol.* **MTT-34** 542–51
- Chato J C 1985 Selected thermophysical properties of biological materials *Heat Transfer in Medicine and Biology, Analysis and Applications* vol 2, ed A Shitzer and R C Eberhart (New York: Plenum) pp 413–18
- Damianou C and Hynynen K 1993 Focal spacing and near-field heating during pulsed high temperature ultrasound therapy *Ultrasound Med. Biol.* **19** 777–87
- Do-Huu J P and Hartemann P 1981 Annular array transducer for deep acoustic hyperthermia *Ultrasonic Symp. Proc. IEEE-81* (New York: IEEE) ch 1689–99, pp 705–10
- Ebbini E and Cain C A 1991a A spherical-section ultrasound phased array applicator for deep localized hyperthermia *IEEE Trans. Biomed. Eng.* **BME-38** 634–43
- 1991b Optimization of the intensity gain of multiple-focus phased-array heating patterns *Int. J. Hypertherm.* **7** 953–73
- Ebbini E S, Umemura S, Ibbini M and Cain C A 1988 A cylindrical-section ultrasound phased-array applicator for hyperthermia cancer therapy *IEEE Trans. Ultrason. Ferroelectr. Freq. Control* **UFFC-35** 561–72
- Fan X 1995 Noninvasive ultrasound surgery using spherically curved phased arrays *PhD Dissertation* University of Arizona
- Fan X and Hynynen K 1992 The effect of wave reflection and refraction at soft tissue interfaces during ultrasound hyperthermia treatments *J. Acoust. Soc. Am.* **91** 1727–36

- Fan X and Hynynen K 1994 The effects of curved tissue layers on the power deposition patterns of therapeutic ultrasound beams *Med. Phys.* **21** 25–34
- 1995 Control of the necrosed tissue volume during noninvasive ultrasound surgery using a 16-element phased array *Med. Phys.* **22** 297–306
- 1996 Ultrasound surgery using multiple sonications—treatment time considerations *Ultrasound Med. Biol.* at press
- Golub G and Kahan W 1965 Calculating the singular values and pseudo-inverse of a matrix *J. SIAM Numer. Anal.* **2** 205–24
- Ocheltree K B, Benkeser P J, Frizzell L A and Cain C A 1984 An ultrasonic phased array applicator for hyperthermia *IEEE Trans. Son. Ultrason.* **SU-31** 526–31
- O’Neil H T 1949 Theory of focusing radiators *J. Acoust. Soc. Am.* **21** 516–26
- Pennes H H 1948 Analysis of tissue and arterial blood temperatures in the resting human forearm *J. Appl. Physiol.* **1** 93–122
- Sapareto S A and Dewey W C 1984 Thermal dose determination in cancer therapy *Int. J. Radiat. Oncol. Biol. Phys.* **10** 787–800
- Yoon Y J 1991 Ultrasonic phased arrays with variable geometric focusing for hyperthermia applications *PhD Dissertation* Georgia Institute of Technology